Numerical study of highly turbulent under-expanded hydrogen jet flames impinging walls

Gallen, L.[1], Sibawayh, S.[2], Louriou, C.[2], Livebardon, T.[2] and Sommerer, Y.[2]

[1] Airbus Protect SAS, 37 Avenue Escadrille Normandie Niemen, 31700 Blagnac, France
lucien.gallen@airbus.com
[2] Airbus Operations SAS, 316 Route de Bayonne, 31300 Toulouse, France

Abstract

Heat flux on walls from under-expanded H2/AIR jet flames have been numerically investigated. The thermal behaviour of a plate close to different under-expanded jet flames has been compared with rear-face plate temperature measurements. In this study, two straight nozzles with millimetric diameter were selected with H2 reservoir pressure in a range from 2 to 10 bar. The CFD study of these two quite different horizontal jet flames employs the Large Eddy Simulation (LES) formalism to capture the turbulent flame-wall interaction. The results demonstrated a good agreement with experimental wall heat fluxes, computed from plate temperature measurements. The present study assesses the prediction capability of LES for flame-wall heat transfer.

Introduction

Recently, hydrogen potential to decarbonize transportation [1] has led to much academic and applied research. Due to hydrogen properties including high flammability, high flame speed, lack of odor and color, most of the research focuses on safety engineering [2]. These properties raise numerous challenges associated with the onboard storage of hydrogen in aircraft to use it as a main fuel. Due to its low volumetric energy density, storing gaseous hydrogen in high-pressurised vessels or in liquid state at a very low temperature in insulated tanks seems to be a promising way to make it available as an energy carrier. However, in the case of unwanted and sudden release from a damaged pressurised storage or distribution system, which is the most common incident [2], hydrogen is released with a high pressure ratio leading to an under-expanded jet [3]. The induced plume is likely to ignite due to hydrogen high-flammability and low ignition energy [4,5]. The resulting flame length can cover a wide range of distances [6,7,8] and may cause heat ingress on surrounding devices and systems. Thus, for supporting the development of reliable and safe hydrogen-based technologies, predictive tools to address the consequences of impinging jet flames shall be developed.

Heat transfer of both non-reacting and reacting impinging jets have been studied for a long time [9,10,11]. Non-reacting impinging jets offer a large range of fundamental physical concepts in basic configuration including large and small scale vortices, wall boundary layers, wall heat transfer and intermittency [12]. For reacting ones, additional physical concepts are involved such as instabilities [13] and flame wall interaction (FWI) [14]. In hydrogen safety related topics, numerous studies on a vertical flame impinging the ceiling [15,16,17] have been carried out to investigate flame morphology under a ceiling. Horizontal impinging jet flames have been experimented by Sandia to evaluate barrier wall configurations [18,19,20] and computed with Computational Fluid Dynamics (CFD) using Reynolds-Averaged Navier-Stokes (RANS) [7]. They investigated flame morphology, thermal radiation, wall shape impact on overpressure, and mitigation. Horizontal under-expanded jet flames impinging a vertical plate has been recently investigated by Wang et al. [21,22], experimental measurements have been conducted under various jet velocity and nozzle-wall spacing. The analysis of flame morphology and spread mechanism have led to a model to predict the flame spreading along the wall accounting for initial momentum of the jet, buoyancy forces and wall resistance force. To the authors knowledge, similar studies focusing on thermal flux induced by a horizontal under-expanded jet flames impinging a vertical material are limited.

In this work, a horizontal jet flame impinging a vertical plate has been experimentally carried out under different conditions varying pressure ratios and nozzle diameters with a constant nozzle-wall

spacing. The experimental study focuses on the thermal behavior of the plate with the evaluation of associated wall heat fluxes. A parallel numerical study is conducted to build a methodology to reproduce experimental results of the impinging under-expanded jet flames. The numerical approach is based on Large Eddy Simulations (LES). , which have become widely used to study turbulent combustion and impinging jet [12,23] and more affordable than Direct numerical simulations (DNS) [24].
The paper is divided into two parts. Both experimental and numerical setup are first described as well as the methodology employed to retrieve wall heat fluxes. Then results are discussed and compared with available experimental measurements.

Experimental setup

Test bench description

For the experimental investigation of the impinging hydrogen flames, a test bench shown in Fig.1 was built at Ineris facilities. The tests were conducted in their ventilated 1000m3 fire room.

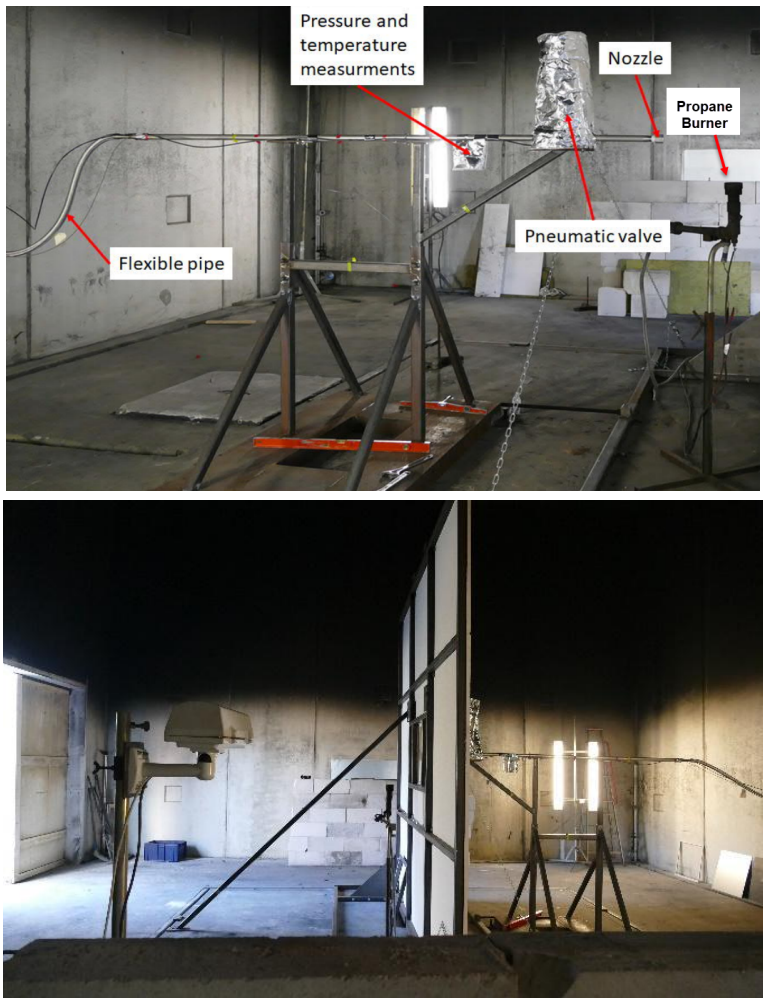

Figure 1: Left: 1000m^3 Fire room - Right: Hydrogen Test Bench.

Just outside of the Fire room are placed Nitrogen bottles and 200bar hydrogen cylinders. The bottles are connected to a set of pressure regulators and bypass valves feeding the test bench in the room through a 1 inch inner diameter flexible pipe. This latter is then connected to a 1 inch inner diameter stainless pipe feeding the millimetric diameter nozzle. Pressure and Temperature transducers are placed upstream the nozzle to monitor the release conditions.

The nozzle used is a Swagelok High pressure Plug for which the schematics are shown in Figure 2. This nozzle (and all the experimental setup) is not meant to represent any standard burner in the eyes of aviation authoroties. Next to the nozzle is a propane burner to ignite the release. The burner is turned on before the hydrogen release and is shut down immediately after ensuring the presence of stabilized hydrogen jet flame (which is usually a few seconds after the opening of the hydrogen valve).

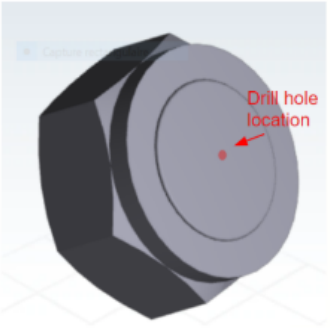

Figure 2: Swagelok High Pressure Plug.

Finally, a support wall is positioned downstream from the nozzle. The wall is lined up with low thermal conductivity insulation. Within the wall is a window on which the impinged plate is placed and secured with a metallic flange at the backside. The same insulation material is used to avoid any direct contact between the flange and the plate.
The impinged specimen is a titanium plate of thickness of 6mm. The plate temperature was recorded using 31 thermocouples (K type, 1mm diameter) placed 2.5mm deep (from its backside) within the plate. The radial distribution of the thermocouple is shown in Figure 3.

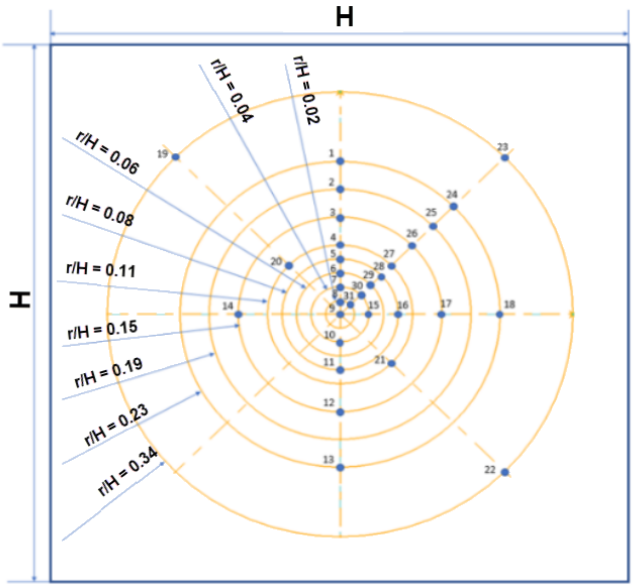

Figure 3: Impinged Plate Thermocouple Distribution.

For this test campaign two flame impinging scenarios were conducted where the pressure and nozzle diameter were varied and reported in Tab. 1.

Table 1. Experimental release conditions

	Nozzle Diameter	Pressure	Nozzle-to-Plate Distance

Test PD_1	D_1 [mm]	5 - 10 bar	100 D_1
Test PD_2	$D_2 = 8\ D_1$ [mm]	2 - 5 bar	12.5 D_2

Experimental measurements and exploitation

The final test setup before igniting the propane burner and starting the hydrogen release is shown in Fig. 4.

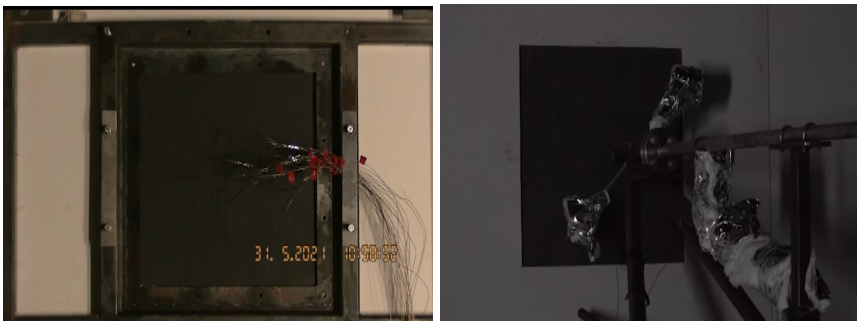

Figure 4: Test setup before ignition Left: Front view - Right: Backside view.

After ignition, the hydrogen release was maintained until the stabilization of the impinged plate thermocouple recordings, i.e. the steady state condition, which took approximately 100s. For test PD_1, the stabilized plate temperature as function of radius is plotted in Fig. 5, where the numbers refer to thermocouples. Cold refers to ambient temperature, while Hot refers to maximum plate temperature.

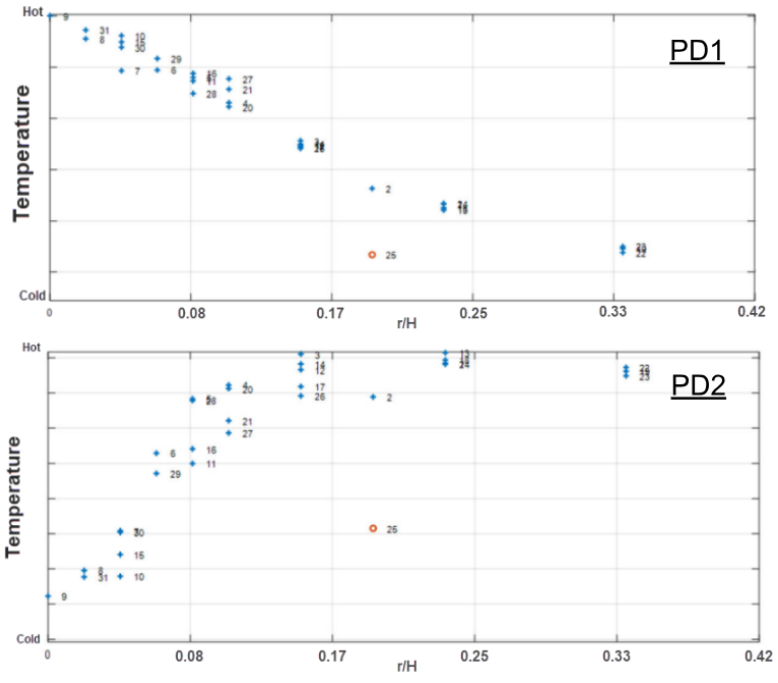

Figure 5: Experimental measured temperatures using TCs along the rear-face of the plate.

For test PD1, the plate temperature presents a maximum at the center and decreases rapidly away from the stagnation point. For Test PD2, the opposite is observed where the plate presents a cold stagnation point. For most of the radii for which several TCs are present, the recorded temperatures are very close owing to an axisymmetric distribution of the plate temperature field. However, some deviation is

observed for some TCs like n°25. This is mainly explained by the fact that the 1mm diameter TCs were inserted, by hand, into 1.1mm diameter holes. This results in a loose contact and uncontrolled thermal contact between the n°25 TCs bead and the plate. The issue with TCs n° 25 occurred on both tests.

In addition to the recorded plate temperature, it was important to identify the heat transfer between hot gas and the impinged plate. This identification has been conducted by ONERA using Beck's inverse method of sequential function estimation built into the solver MODETHEC[25,26,27]. The inverse method is a mathematical constrained optimization problem that aims at identifying unknown parameters (in this case the surface heat flux) using direct temperature measurements.. The boundary conditions setup for the inverse method application is shown in Figure 8. As mentioned above, the plate has been insulated to limit conductive heat loss to the test bench support. As such, the lateral surfaces of the plate were assumed adiabatic. On the backside of the plate, the heat dissipation by natural convection and radiation are modelled respectively by

$$q_{conv} = h\left(T_w - T_\infty\right) \quad (1)$$

and,

$$q_{rad} = \varepsilon\sigma\left(T_w^4 - T_\infty^4\right). \quad (2)$$

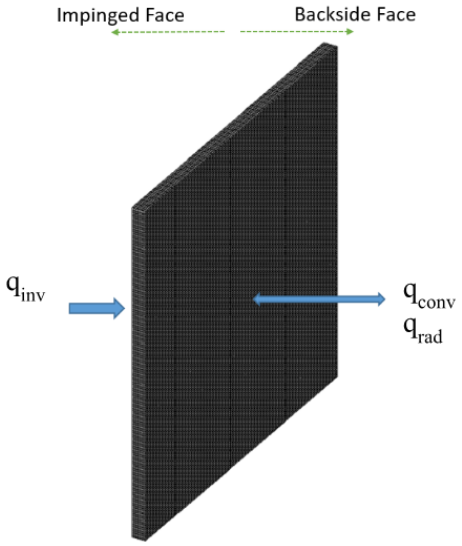

Figure 6: MODETHEC Thermal model boundary conditions.

Where ε is the impinged plate emissivity, T_{plate} the experimentally measured TC data, $T_{ambient}$ the ambient temperature and h the convective heat transfer coefficient. The output of the MODETHEC solver is the impinged face heat flux density q_{inv} which will be compared numerically with the predicted wall heat flux in Fig. 12

Numerical setup

Numerical strategy

The LES code AVBP (www.cerfacs.fr/avbp7x/) developed by CERFACS, the numerical schemes and subgrid-scale model for impinging jets are described in Aillaud et al. [12]. Hydrogen-air chemistry is described with the semi-detailed SanDiego chemical [28] that comprises 9 transported species and 21 reactions. All computations are 3D and the mesh used is a hybrid mesh composed of tetrahedrals and 10 layers of prisms on the plate. It contains about 20M cells with specific refinement in the nozzle (Δx =50µm) in flame (Δx =700µm) and in the near wall region with $1 < y^+ < 5$.

Computational domain and boundary conditions are illustrated in Fig. 7. Hydrogen inlet mass flow rate and outlet pressure are imposed using the NSCBC formalism [29]. A small coflow at atmospheric conditions is imposed far upstream to ensure computation stability without impacting the impinging jet since $U_{coflow} << 0.05\ U_{jet\ bulk\ velocity}$ [12]. The nozzle is a no-slip isothermal wall (set to ambient temperature) to prevent flame anchoring to the nozzle. For the plate, a zero mass-flux boundary condition with zero-velocity is used, where the wall normal heat flux at iteration (n+1) is formulated as:

$$q^{n+1} = -\frac{T^{n}_{wall} - T_{ref}}{R_{th}} \quad \text{with} \quad R_{th} = \frac{plate\ thickness, e}{plate\ thermal\ conductivity, k} = 9.0\ e^{-4} \tag{3}$$

where T_{wall} [K] is the wall temperature, T_{ref} [K] is the rear-face plate temperature and the heat resistance R_{th} [K m^2 W^{-1}] is determined considering conduction in the plate. Plate thermal conductivity is fixed at low temperature to reproduce maximum heat flux on the plate. This boundary condition aims to mimic the thermal behavior of the plate without CHT which is necessary to capture the good flame morphology. For case PD_2, the computational domain is enlarged by a factor 3 due to higher turbulence with a stronger impinging jet flame.

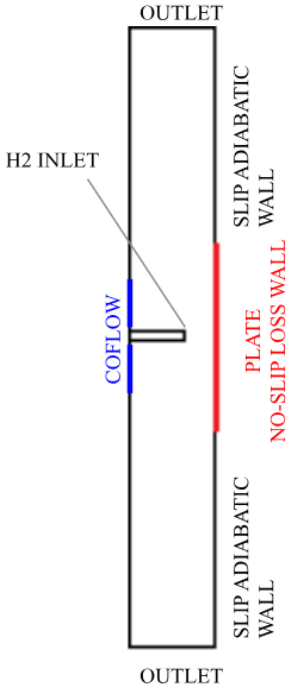

Figure 7: sketch of the computational domain

Discussion

Flow topology

Cases PD_1 and PD_2 lead to very different flow topology, this part aims to analyse and compare the flow field impacting the vertical plate. Figure 8 highlights these differences showing the mean numerical schlieren computed for both cases. Based on the detailed review of Franquet et al. [30], Case PD_1 exhibits a barrel shock indicating a highly under-expanded jet while case PD_2 exhibits a very flat diamond shock structure typical of moderate under-expanded jet, at the limit of adapted jets which are subsonic.

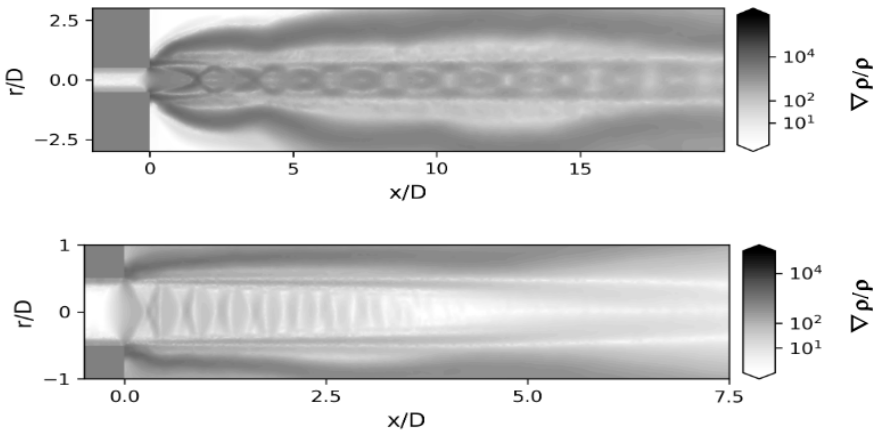

Figure 8: Mean field of numerical Schlieren for cases PD_1 (top) and PD_2 (bottom).

The mean Mach number of each jet is analyzed in Fig. 9. The supersonic zone is highlighted by a black isoline Mach = 1. Supersonic zone widths are proportional to the nozzle diameter, significantly different between PD_1 and PD_2. While the magnitude of the Mach number inside the supersonic zone is much higher in PD_1 than PD_2, levels of Mach number in the transition zone, at the end of the supersonic zone, are similar. However the jet opening is much higher for PD_2. It is important to note that the plate is located at 100D for PD_1 and 12.5D for PD_2. Considering the nozzle-wall length L, the supersonic length of PD_1 is about L/4 while it is about L/2 for PD_2. Although the PD1 pressure ratio is higher, the PD_2 pressure ratio/nozzle diameter combination leads to higher impinging velocity on the plate.

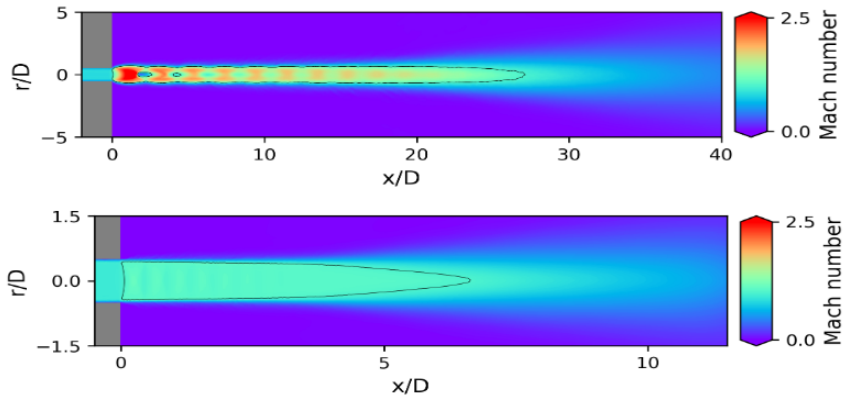

Figure 9: Mean field of Mach number for cases PD_1 (top) and PD_2 (bottom).

Flame topology

Flame topology is investigated for both cases in Fig. 10. Mean field of temperature indicates two very different impinging flow reacting patterns. In both cases flame is stabilized on the nozzle, due to a small nozzle-wall distance L flame spreading on the plate is observed. For PD_1, maximum temperature is located at the stagnation point and flame exhibits an envelope flame shape [10]. Contrary to PD_1, the impinging jet is stronger and the radial flow velocity of the impinging jet is high as shown by the streamlines plotted in Fig. 10. It leads to a cool central core flame which is an envelope flame characterized by a cold core at the stagnation point. Maximum temperature and then heat fluxes are expected further in the radial direction. After reaching the maximum temperature in the near-wall region, flow topology indicates that hot pockets of burnt gas are ejected from the plate in opposite axial directions. Such loss of temperature distribution spreading along the plate should lead to a

significant decrease in global heat fluxes. Note that no buoyancy effect is observed in these two momentum-driven under-expanded jets.

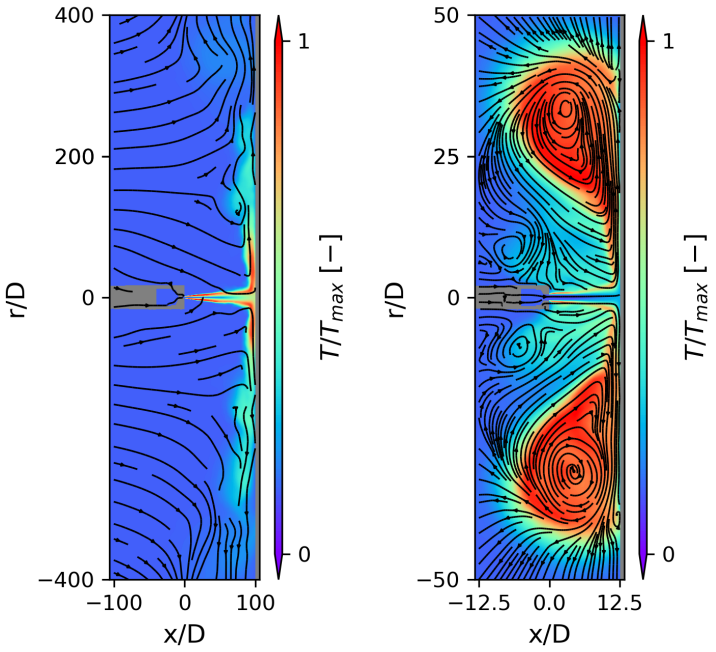

Figure 10: Mean field of temperature for case PD_1 (left) and PD_2 (right) with black streamlines.

Instantaneous temperature distributions on the plate are presented in Fig. 11. Identified flame patterns are assessed with this direct visualization of the flame spreading. The envelope flame observed in PD_1 leads to a small flame spreading, with a strong accumulation of hot gas at the stagnation point. However the cool central core flame observed in PD_2 leads to a small cold region at the stagnation point, then temperature is maximal before decreasing as the hot gas are ejected from the plate.

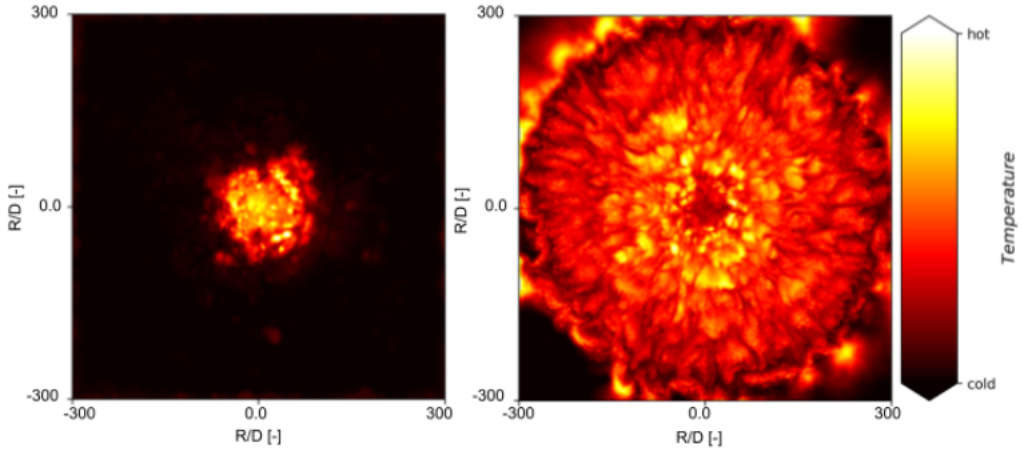

Figure 11: Instantaneous field of plate temperature for case PD_1 (left) and PD_2 (right).

Wall heat fluxes prediction

The associated wall heat fluxes of case PD_1 and PD_2 are presented in Fig. 12. For both cases, a good agreement is observed between the inverse heat flux computed from experimental plate temperature measurements, q_{inv} and the wall heat flux obtained with LES, q_{LES}. Both magnitude and shape of q_{inv} are retrieved from the LES. For case PD_1, q_{LES} captures good magnitude at the stagnation point as well as the R>100 zone, between them the shape is retrieved but with a spatial shift. In PD_2, the radial evolution of wall heat flux q_{LES} is in agreement with the envelope shape of the flame with a cool central core discussed in the flame topology part. Radial evolutions of wall heat flux are in a good agreement with q_{inv} for PD_2. The small heat flux at the stagnation point close to R = 0 in (I) is correctly retrieved as well as the peak location of heat flux in the end of (I). Fluctuations and shape in (II) where the flame is located with turbulence is as well reproduced. In LES, the flame is slightly ejected from the plate by the jet topology and then heat fluxes decrease slowly in (III) while q_{inv} is measured higher and quasi constant in this zone. It suggests that the experimental flame spreading along the plate goes a bit further radially (III). However flame spreading is very similar in both cases PD_1 and PD_2.

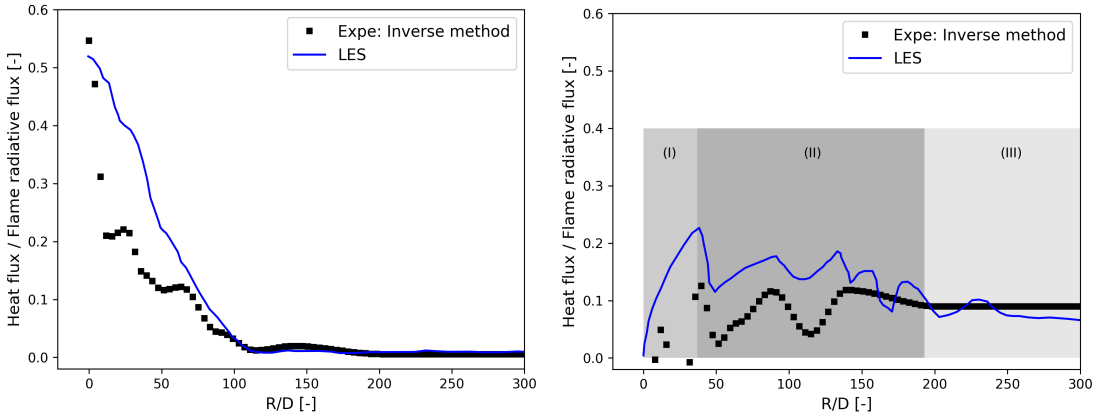

Figure 12: Spatial mean of wall heat flux along the radial direction of the plate. Comparison between experimental and numerical heat fluxes for PD_1 (left) and PD_2 (right).

Figure 13 assesses the influence of wall boundary conditions on the flame pattern. Case PD_1 has been investigated with several no-slip boundary conditions, respectively adiabatic, isothermal at 290K and using the heat loss used in this work. A very strong impact is observed on the flame spreading along the plate. As expected, in the adiabatic case, the flame spreading is maximum meaning both flame and hot burnt gas propagate radially along the plate. For the isothermal case, flame spreading doesn't exceed the flame the jet width, flame is then ejected from the plate in the opposite direction. It confirms that, for such small wall-nozzle length, the wall temperature drives the flame topology.

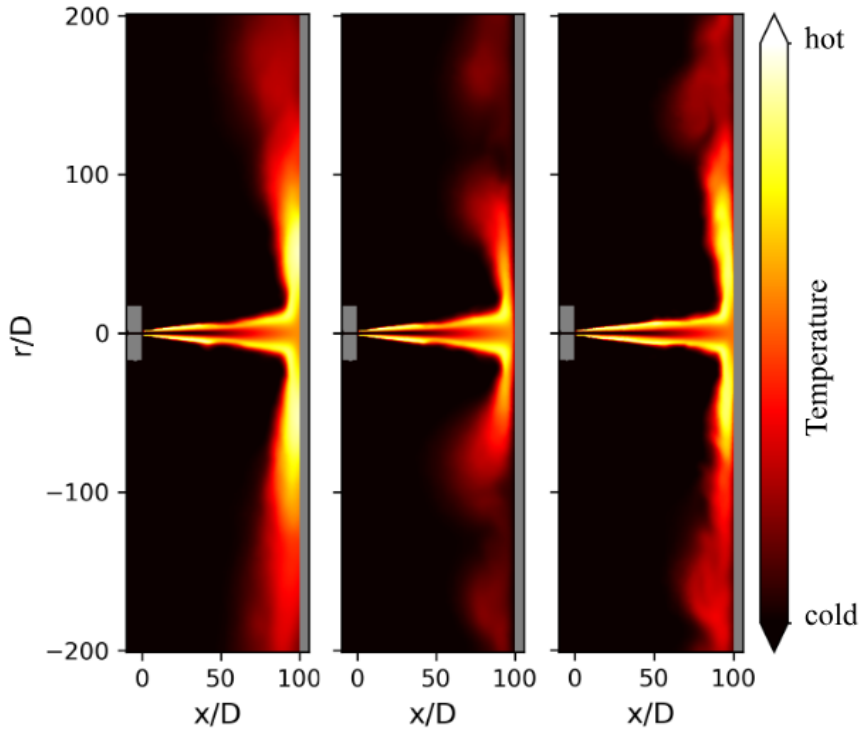

Figure 13: Comparison of mean field of temperature for case PD_1 using adiabatic plate (left), cold isothermal plate (center) and heat loss plate (right).

Conclusions

Both experimental and numerical under-expanded jet flames covering various diameters and pressures and impacting metallic plates have been investigated. The use of realistic-like boundary conditions for the plate gives a good agreement with the experimental wall heat fluxes obtained with the inverse method from thermocouples located at the rear face of the plate. Heat loss boundary condition has been tested to predict wall heat flux and then flame spreading along the plate. In this study, LES demonstrates its capability to predict wall heat flux for very different under-expanded jet flames without a use of conjugate heat transfer (CHT) approach. This assessment is very promising as such an approach requires additional effort in computational setup and CPU requirements. However, LES-based CHT methodology seems to be inescapable for addressing complex systems impacted by flames, eased by the democratization of computing resources [31,32]. The next step is then to evaluate the proposed approach and CHT methodology to address complex and representative heat flux problems dealing with under-expanded jet flame. Moreover, it is worth noting that the test bench used for this paper is not transposable to an aircraft scenario as no burner standard is defined for hydrogen by national aviation authorities

Acknowledgements

The authors gratefully acknowledge CERFACS for their support to use the LES solver AVBP and their insights. The authors would also like to thank and acknowledge the contribution of Ineris for their valuable support for the experimental test campaign setup and realisation. Finally, the authors would like to express their thanks to ONERA for their support in the wall heat flux identification. Funding from Airbus, DGAC and the European Union within the project NextGenerationEU is gratefully acknowledged.

References

[1] Dunn, S. “Hydrogen futures: toward a sustainable energy system.” International Journal of Hydrogen Energy, vol. 27, no. 3, 2002, pp. 235-264.
[2] Yang, F., Wang, T., Deng, X., Dang, J., Huang, Z., Hu, S., Li, Y. and Ouyang, M. “Review on hydrogen safety issues: Incident statistics, hydrogen diffusion, and detonation process.” *International Journal of Hydrogen Energy*, vol. 46, no. 61, 2021, pp. 31467-31488.
[3] Han, S. H., Chang, D. and Kim, J.S. “Experimental investigation of highly pressurized hydrogen release through a small hole.” *Experimental investigation of highly pressurized hydrogen release through a small hole*, vol. 39, no. 17, 2014, pp. 9552-9561.
[4] Adamson, K.A. and Pearson, P. “Hydrogen and methanol: a comparison of safety, economics, efficiencies and emissions.” Journal of Power Sources, vol. 86, no. 1-2, 2000, pp. 548-555.
[5] Xu, B. P., Wen, J.X., Dembele, S., Tam, V.H. and Hawksworth, S.J. “The effect of pressure boundary rupture rate on spontaneous ignition of pressurized hydrogen release.” Journal of Loss Prevention in the Process Industries, vol. 22, no. 3, 2009, pp. 279-287.
[6] Schefer, R. W. “Spatial and radiative properties of an open-flame hydrogen plume.” International Journal of Hydrogen Energy, vol. 31, 2006, pp. 1332-1340.
[7] Houf, W. G., Evans, G.H. and Schefer, R.W. “Analysis of jet flames and unignited jets from unintended releases of hydrogen.” International Journal of Hydrogen Energy, vol. 34, no. 14, 2009, pp. 5961-5969.
[8] Schefer, R. W., Houf, W.G., Williams, T.C., Bourne, B. and Colton, J. “Characterization of high-pressure, underexpanded hydrogen-jet flames.” International Journal of Hydrogen Energy, vol. 32, 2007, pp. 2081-2093.
[9] Hrycak, P. “Heat transfer from round impinging jets to a flat plate.” International Journal Heat Mass Transfer, vol. 26, no. 12, 1983, pp. 1857-1865.
[10] Zhang, Y. and K.N C. Bray. “Characterization of Impinging Jet Flames.” Combustion and Flame, vol. 116, 1998, pp. 671-674.
[11] Foat, T., Yap, K.P., and Zhang, Y. “The visualization and mapping of turbulent premixed impinging flames.” Combustion and Flame, vol. 125, no. 1-2, 2001, pp. 839-851.
[12] Aillaud, P., Duchaine, F and Gicquel, L.Y.M. “Secondary peak in the Nusselt number distribution of impinging jet flows: A phenomenology analysis.” Physics of Fluids, vol. 28, no. 9, 2016, pp. 095-110.
[13] Schuller, T., Durox, D. and Candel, S. “Dynamics of and noise radiated bya perturbed impinging premixed jet flame.” Combustion and Flame, vol. 128, 2002, pp. 88-110.
[14] Dabireau, F., Cuenot, B., Vermorel, O., and Poinsot, T. “Interaction of flames of H2+O2 with inert walls.” Combustion and Flame, vol. 135, no. 1-2, 2003, pp. 123-133.
[15] Ding, H. and J. G. Quintiere. “An integral model for turbulent flame radial lengths under a ceiling.” Fire Safety Journal, vol. 52, 2012, pp. 25-33.
[16] Zhang, X., Hu, L., Zhu, W., Zhang, X. and Yang, L. “Flame extension length and temperature profile in thermal impinging flow of buoyant round jet upon a horizontal plate.” Applied Thermal Engineering, vol. 73, 2014, pp. 15-22.
[17] Gao, Z., Ji, J., Wan, H., Li, K. and Sun, J. “An investigation of the detailed flame shape and flame length under the ceiling of a channel.” Proceedings of the Combustion Institute, vol. 35, 2015, pp. 2657-2664.
[18] Schefer, R. W., Groethe, M., Houf, W.G. and Evans, G.H. “Experimental evaluation of barrier walls for risk reduction of unintended hydrogen releases.” International Journal of Hydrogen Energy, vol. 34, 2009, pp. 1590-1606.
[19] Schefer, R. W., Merilo, E.G., Groethe, M.A. and Houf, W.G. “Experimental investigation of hydrogen jet fire mitigation by barrier walls.” International Journal of Hydrogen Energy, vol. 36, no. 3, 2011, pp. 2530-2537.
[20] Houf, W.G. and Schefer, R.W. “Predicting radiative heat fluxes and flammability envelopes from unintended releases of hydrogen.” International Journal of Hydrogen Energy, vol. 32, 2007, pp. 136-151.

[21] Wang, C., Ding, L., Wan, H. and Ji, J. “Experimental study of flame morphology and size model of a horizontal jet flame impinging a wall.” Process Safety and Environmental Protection, vol. 147, 2021, pp. 1009-1017.
[22] Wang, Z., Jiang, J., Wang, G., Ni, L., Pan, Y. and Li, M. “Flame morphologic characteristics of horizontally oriented jet fires impinging on a vertical plate: Experiments and theoretical analysis.” Energy, vol. 264, 2023.
[23] Pantangi, P., Sadiki, A., Janicka, J., Mann, M. and Dreizler, A “LES of premixed methane flame impinging on the wall using non-adiabatic flamelet generated manifold (FGM).” Flow, turbulence and combustion, vol. 82, 2014, pp. 805-836.
[24] Ranga Dinesh, K K J., Jiang, X. and van Oijen, J.A. “Numerical simulation of hydrogen impinging jet flame using flamelet generated manifold reduction.” International Journal of Hydrogen Energy, vol. 37, no. 5, 2012, pp. 4502-4515.
[25] Biasi, V. Modélisation thermique de la dégradation d'un matériau composite soumis au feu. PhD Thesis. ISAE, 2014.
[26] Reulet, P., Nortershauser, D. and Millan, P. “Inverse Method Using infrared Thermography for Surface Temperature and Heat Flux Measurements”, Proceedings of the International Congress on Instrumentation in Aerospace Simulation Facilities, Vol. 1, pp. 118–126, 2003.
[27] Pichillou, J., Grenard, P., Vingert, L., Leplat, G. and Reulet, P. “Experimental analysis of heat transfer in cryogenic combustion chambers on Mascotte test bench”, 7th European Conference for Aeronautics and Space Sciences (EUCASS), Milan Italy, 2017.
[28] Saxena, P. and F. Williams. “Testing a small detailed chemical-kinetic mechanism for the combustion of hydrogen and carbon monoxide.” *Combustion and Flame*, vol. 145, 2006, pp. 316-323.
[29] Poinsot, T. and Lele, S. “Boundary conditions for direct simulations of compressible viscous flows.” Journal of Computational Physics, vol. 101, no. 1, 1992, pp. 104-129.
[30] Franquet, E., Perrier, V., Gibout, S. and Bruel, P. “Free underexpanded jets in a quiescent medium: A review.” *Progress in Aerospace Sciences*, vol. 77, 2015, pp. 25-53.
[31] Boulet, L., Benard, P., Lartigue, G., Moureau, V., Chauvet, N. and Duchaine, F. “Modeling of conjugate heat transfer in a kerosene/air spray flame used for aeronautical fire resistance tests.” Flow, Turbulence and Combustion, vol. 101, 2018, pp. 579-602.
[32] Xu, B. P., Cheng, C.L. and Wen, J.X. “Numerical modelling of transient heat transfer of hydrogen composite cylinders subjected to fire impingement.” International Journal of Hydrogen Energy, vol. 44, no. 21, 2019, pp. 11247-11258.